

Visualization and orbital-free parametrization of the large- Z scaling of the kinetic energy density of atoms

Antonio C. Cancio¹ and Jeremy J. Redd²

¹*Department of Physics and Astronomy, Ball State University, Muncie, Indiana 47306**

²*Department of Physics, Utah Valley University, Orem, Utah 84058**

The scaling of neutral atoms to large Z , combining periodicity with a gradual trend to homogeneity, is a fundamental probe of density functional theory, one that has driven recent advances in understanding both the kinetic and exchange-correlation energies. Although research focus is normally upon the scaling of integrated energies, insights can also be gained from energy densities. We visualize the scaling of the positive-definite kinetic energy density (KED) in closed-shell atoms, in comparison to invariant quantities based upon the gradient and Laplacian of the density. We notice a striking fit of the KED within the core of any atom to a gradient expansion using both the gradient and the Laplacian, appearing as an asymptotic limit around which the KED oscillates. The gradient expansion is qualitatively different from that derived from first principles for a slowly-varying electron gas and is correlated with a nonzero Pauli contribution to the KED near the nucleus. We propose and explore orbital-free meta-GGA models for the kinetic energy to describe these features, with some success, but the effects of quantum oscillations in the inner shells of atoms makes a complete parametrization difficult. We discuss implications for improved orbital-free description of molecular properties.

Keywords: Density Functional Theory, Kinetic Energy Density, orbital-free DFT, meta-GGA, Thomas-Fermi Theory

I. INTRODUCTION

The basic insight of density functional theory (DFT) [1] is that the ground state energy and related quantities are functionals of the particle density alone. Historically, however, functionals have nearly always been implemented in the Kohn-Sham approach which uses auxiliary orbitals derived from the solution to an equivalent effective noninteracting problem. Orbitals prove very important to describe features in the kinetic energy such the effect of the quantum oscillations of the shell structure of atoms. However, the project of developing a true orbital-free DFT, using the density only to obtain energies and electronic structure remains a challenge. This challenge has taken on new impetus with the demand for applications in which the use of orbitals is prohibitive [2]. Such situations include the simulation of mesoscale systems [3] and of warm dense matter [4, 5] – matter at high density, at temperatures roughly of the fermi temperature, where a macroscopic portion of electrons are thermally excited. Given robust orbital-free models of exchange and correlation in the form of generalized gradient approximations (GGA's) [6–8], there remains an ongoing need for developing improved orbital-free models of the Kohn-Sham kinetic energy (KE).

Much work in this area [9–14] has centered on development of GGA's for the KE – corrections to the Thomas Fermi approximation [15, 16] constructed from the local density and its gradient. These include nonempirical or semi-nonempirical models based on the satisfaction of exact constraints [9, 11]. A common but not always ac-

curate [17] design principle is that of conjointness with exchange [18] – the development of forms that can be adapted to describe both exchange and kinetic energies. A second area of research is the construction of nonlocal or two-point functionals, which incorporate quantum oscillations such as Friedel oscillations and shell structure at the cost of a nonlocal dependence upon density [19–23] These have had success for very large solid-state applications [24, 25], but rely upon material-dependent functionals.

The goal of this paper is to bring together two disparate themes in density functional theory and bring them to bear upon the problem of orbital-free functionals.

The first is as old as density functional theory itself – the large- Z limit of the neutral atom. As one proceeds down the periodic table, increasing both nuclear charge Z and electron number N to maintain charge neutrality, and allowing both to increase indefinitely, one gradually turns off the effects of inhomogeneity on the quantum many-body system in a quantifiable way. The infinite- Z limit for both density and energy is given exactly [26, 27] by the Thomas-Fermi model of the atom [15, 16, 28], – a semiclassical solution that is essentially a completely orbital-free local density approximation. The general trend of corrections to this picture as Z is brought down to realistic values has also long been known [29–31], leading to a series expansion in $1/Z^{1/3}$. These corrections include gradient corrections to the kinetic energy [32, 33] as well as the introduction of exchange and correlation corrections [34–36] as both vanish relative to the KE as $Z \rightarrow \infty$. At even lower values of Z , atoms like third-row transition metals provide open challenges to traditional DFT approaches like GGA's and meta-GGA's (function-

* accancio@bsu.edu

als that use a third variable, either the Laplacian of the density or the KED in addition to the local density and its gradient [36, 37].) This scaling thus serves as a natural, disciplined way to study the gradual introduction of inhomogeneity into density functionals. Essentially, to ascend to large- Z is tantamount to descending the Jacob’s Ladder of functionals from complicated orbital-dependent ones to the local-density approximation.

However, it is only fairly recently that the implications of this scaling behavior have made their way explicitly into density functional development. Work has been done in improving the understanding of the connection between the large- Z scaling of atomic energies and density functional theory [35–40] and along the way, developing new functionals for the kinetic energy [11, 39, 41, 42], exchange [11, 38, 42], and most recently, correlation [36, 37].

The other theme in DFT development that we will explore exploits the modeling of the Kohn-Sham kinetic energy density – the contribution to the KS KE on a point-by-point basis. The KED is an important measure of electronic structure first of all in a qualitative sense – as the basis for the electron localization factor or ELF [43, 44] that identifies regions of electron localization such as atomic shells and covalent bonds from regions with localized electrons. It is also the key ingredient in meta-GGA’s [45, 46] – where the ELF’s ability to diagnose different types of bonds can be used to construct functionals that work well for a large variety of systems. Recent work on the orbital-free modeling of the KED, and thus implicitly the ELF [47–53] demonstrates that the gradient and Laplacian of the density taken together can be used to construct effective meta-GGA functionals of the KE density. This approach has the promise of bringing the insights into electronic structure gained from the ELF to the context of OFDFT development.

This paper is an attempt to combine these two complementary approaches. Although the KE density of atoms has been the subject of numerous studies [40, 48, 54, 55], little has been done to visualize and analyze their scaling properties as $Z \rightarrow \infty$. An issue of interest is how different regions of the atom scale with Z . There should be a contrast between the interior of the atom where the shell structure that characterizes finite atoms tends to the smooth Thomas-Fermi limit and the near-nuclear core and classically forbidden tunnelling region far from the nucleus, both of which never converge to the Thomas-Fermi limit. Particularly, the universal limiting behavior of the KED in these regions could offer important guidance for functional development as they provide important boundary conditions that those functionals should try to meet. A related question is why the gradient expansion works as well as it does [56] for these systems despite the significant departures from homogeneity in the valence shell and at the nucleus.

In this paper we discuss preliminary results of the visualization of scaling behavior of the gradient and Laplacian of the density as a function of Z , and of the Kohn-Sham KED as a function of these quantities. We show

that there are at least two types of scaling behavior as Z tends to ∞ , a highly nonanalytic behavior describing the near-nuclear region, and the other describable by an empirical gradient expansion in the rest of the atom. Notably, the empirical gradient expansion is different from that canonically derivable from the slowly-varying electron gas, and thus from that used in most GGA and meta-GGA functionals. This difference may have significant impact on the ability of these functionals to predict binding in molecules. The rest of this paper is organized as follows: Sec. II describes the theoretical background of the paper – the density functional theory of the kinetic energy density, and in particular in the context of the atomic problem. Sec. III covers the basic methodology used for calculations. Sec. IV details the chief results of visualization, and their implications for the total energy of atoms and Sec. V presents a discussion of these results and our conclusions.

II. THEORY

The kinetic energy density in Kohn-Sham theory is given by

$$\tau_{KS} = \frac{1}{2} \sum_i^{occup} f_i |\nabla \phi_i|^2, \quad (1)$$

where ϕ_i are Kohn-Sham orbitals from which the electron density is constructed:

$$n = \sum_i^{occup} f_i |\phi_i|^2, \quad (2)$$

and f_i is the occupation number of each orbital. Integration over all space gives the kinetic energy

$$T_{KS}[n] = \int \tau_{KS}(\mathbf{r}) d^3r. \quad (3)$$

A generalization in terms of the spin density and spin-decomposed KED’s may be constructed by restricting the sums in the equations above to a specific spin species. An alternative KED, completely equivalent to Eq. (1), is

$$\tau'_{KS} = -\frac{1}{2} \sum_i^{occup} f_i \phi_i^* \nabla^2 \phi_i = \tau_{KS} - \frac{1}{4} \nabla^2 n. \quad (4)$$

Note that the difference is the divergence of a vector function, whose integral is zero, leaving the integrated KE unchanged. Eq. (1) however is conveniently positive-definite.

A key principle is that τ_{KS} , like any other property of an electronic system, is a functional of the ground state electron density n . At the same time, this functional relationship can only be approximated. A “semilocal” approximation to $T_{KS}[n]$ defines τ_{KS} at some position \mathbf{r} in

terms of the local density, density gradient and possibly its Laplacian:

$$T_{KS}^{approx}[n] = \int \tau^{approx}[n(\mathbf{r}), \nabla n(\mathbf{r}), \nabla^2 n(\mathbf{r})] d^3r \quad (5)$$

[9, 10, 12–14, 53]. Another approach, not considered here, involves nonlocal functionals with integrals over two spatial variables [19–22, 56].

The lowest level of semilocal functional – the equivalent to the LDA in XC functionals – is the Thomas-Fermi model,

$$\tau_{TF} = \frac{3}{10} k_F^2 n \sim n^{5/3}, \quad (6)$$

with $k_F = (3\pi^2 n)^{1/3}$ the fermi wavevector of the homogeneous electron gas. At a next level of approximation is the gradient expansion (GEA): [57, 58]

$$\tau_{GEA} = \tau_{TF} + \frac{1}{72} |\nabla n|^2 / n + \frac{1}{6} \nabla^2 n + O(\nabla^4). \quad (7)$$

Terms up to fourth [59] and sixth order [60] in this expansion are known.

As is the case with exchange, it is natural to recast the derivatives of the density into scale-invariant quantities, here defined as

$$p = \frac{|\nabla n|^2}{4k_F^2 n}, \quad (8)$$

$$q = \frac{\nabla^2 n}{4k_F^2 n}. \quad (9)$$

Then the GEA becomes

$$\tau_{GEA} = \left[1 + \frac{5}{27} p + \frac{20}{9} q \right] \tau_{TF}, \quad (10)$$

and any generalization of it that preserves the proper scaling of T_{KS} under the uniform scaling of the charge density is constructable from an enhancement factor $F_S(p, q)$ such that

$$\tau_{semilocal} = F_S(p, q) \tau_{TF}. \quad (11)$$

Note however even higher order derivatives than $\nabla^2 n$ may be considered [61], but may prove impractical in applications. The enhancement factor F_S for the kinetic energy plays a role equivalent to that for exchange, F_X , with $E_X \sim F_X e^{LDA}$ being the equivalent construction. The similarities are strong enough to posit a “conjointness conjecture” [18], that the two enhancement factors F_S and F_X are nearly identical.

For the KED, the most crucial issue for large inhomogeneity $p, q \gg 1$ is the limit of the one- or two-particle spin-singlet system. In this case the Kohn-Sham KED reduces to the von Weizsäcker [62] functional:

$$\tau_{vW} = \frac{1}{8} \frac{|\nabla n|^2}{n}, \quad (12)$$

the exact result for a system of N particles obeying Bose statistics and having the density $n(\mathbf{r})$. The KED needed to create $n(\mathbf{r})$ with fermions, the energetic cost of Pauli exclusion, is given by the difference between the Kohn-Sham and von Weizsäcker KED’s

$$\tau_{Pauli} = \tau_{KS} - \tau_{vW} \quad (13)$$

from which one can define a Pauli enhancement factor:

$$F_{Pauli} = \frac{\tau - \tau_{vW}}{\tau_{TF}}, \quad (14)$$

which must hold true for both τ_{KS} or τ^{approx} . The Pauli enhancement factor is positive definite:

$$F_{Pauli} \geq 0 \quad (15)$$

because of the positive cost of Pauli exclusion [63]. Moreover, the response of the fermionic system with respect to changes in density must be larger than that of the Bose system: the Pauli potential $\delta T_{Pauli}(\mathbf{r}) / \delta n(\mathbf{r}) \geq 0$ [64].

Notably, this von Weizsäcker lower bound [Eq. (15)] is not respected by the GEA. The enhancement factor for τ_{vW} is $F_S^{vW} = 5p/3$ which gives it a coefficient to p that is nine times larger than that of the GEA. The resulting Pauli enhancement factor is

$$F_{Pauli}^{GEA} = 1 + \frac{20}{9} q - \frac{40}{27} p \quad (16)$$

For $q=0$, (or alternately, dropping the term proportional to q as is done in GGA’s) $\tau_{GEA} < \tau_{vW}$ for the relatively modest value of $p=27/40$.

We note here that the gradient expansion correction that is linear in q integrates identically to zero. Thus q will only affect energy expectations to fourth order in the gradient expansion. The simplest semilocal functionals normally then are constructed as generalized functions of the remaining variable p – generalized-gradient approximations or GGA’s. These can draw upon a long experience in developing GGA’s for exchange and are easy to implement. The problem is that, even more so than with exchange, functionals at this level are not flexible enough to be competitive with orbital-dependent models. Two recent GGA take complementary approaches to address this situation. The APBE [11], based on the conjointness conjecture [18] takes nearly identical forms for the exchange and kinetic energy enhancement factor, and fit both to the large- Z expansion of atoms to a high degree of accuracy. This takes advantage of a powerful tool – the scaling of atoms to high- Z is an instance of Lieb-Simon scaling [26] in which the effects of inhomogeneity in a finite system are turned off in a controlled fashion. Quite possibly this is an ideal way to construct a GGA [11, 35, 36]. The cost of conjointness however, is to break the von Weizsäcker bound for any finite- Z atom. The VT84F [9] imposes both the slowly-varying gas limit for small p and is limited at large p to $F_{Pauli}(p) > 0$ which guarantees the von Weizsäcker bound. Possibly more importantly, it guarantees the positive-definite bound on

the Pauli potential. It has generally however a poor prediction of total KE's [47].

A natural way around the problem of conflicting constraints is to put the extra degree of freedom q back into the functional, that is, to create a meta-GGA. An instructive attempt is the Perdew-Constantin mGGA [53], which was developed explicitly to model the kinetic energy density, as a replacement for the KED in meta-GGA-level XC functionals. It starts from a conventional meta-GGA exact up to fourth order in the gradient expansion (the GE4-M) to describe the slowly varying limit. In order to impose the von Weizsäcker bound in the limit of strong electron localization, it interpolates between this functional and the von Weizsäcker form using a non-analytic but smooth function of the difference between the enhancement factors $z = F_S^{GE4-M} - F_S^{vW}$. Despite an attractive design philosophy, the mGGA has deficiencies as a practical tool for OFDFT [10, 41, 47]. However, it is of value as an approach for thinking about OFDFT – building from the basis of the kinetic energy *density* which is an important tool for visualization and quantitative modeling of electronic structure.

Along these lines, perhaps the most physically significant role played by the KED in a meta-GGA is as a measure of electron localization [45, 46, 65]. This is done by taking the ratio of the Pauli contribution to the Kohn-Sham KED to that of the Thomas-Fermi model,

$$\alpha = \frac{\tau_{KS} - \tau_{vW}}{\tau_{TF}}. \quad (17)$$

In regions where the KE density is determined predominantly by a single molecular orbital, τ_{KS} approaches τ_{vW} and $\alpha \rightarrow 0$. This limit describes single covalent bonds and lone pairs, and generally situations in which the self-interaction errors in the GGA and LDA are most acute. The homogeneous electron gas, and presumably systems formed by metallic bonds, corresponds to $\tau_{KS} = \tau_{TF}$, $\tau_{vW} \sim 0$ and $\alpha \sim 1$. Between atomic shells and at low density one finds $\alpha \gg 1$, tending to ∞ for an exponentially decaying density if τ_{Pauli} vanishes more slowly than $n^{5/3}$. This limit can be used to detect weak bonds such as van-der-Waals interactions and define interstitial regions in semiconductor systems. The information on the local environment can then be used to customize gradient approximations for specific subsystems [46]. The electron localization factor or ELF [43, 44] is often used in visualization as it converts α into a function with a range between zero and one:

$$\text{ELF} = \frac{1}{1 + \alpha^2}. \quad (18)$$

Note that the different contexts developing meta-GGA's and OFDFT's hides an important fact: $F_{Pauli} = \alpha$ for the true Kohn-Sham enhancement factor. Thus developing an OFDFT is essentially the same problem for both kinetic and exchange-correlation energies – that of modeling an orbital-free ELF.

In recent work [47] we proposed to revise the mGGA following two simple points: imposing the von Weizsäcker

lower bound $\tau_{KS} > \tau_{vW}$ and relying on the second-order gradient expansion otherwise. This satisfies the constraints for the two main limiting cases of the KED – that of delocalized electrons with slowly-varying density and that of strong electron localization, and otherwise keeps physically reasonable behavior for classically forbidden regions with high inhomogeneity. We defined a measure of electron localization z as

$$z = F_S^{GEA} - F_S^{vW} - 1 = \frac{20}{9}q - \frac{40}{27}p, \quad (19)$$

which in a sense can be thought of as an orbital-free expression for α .

A suitable nonanalytic transition between F_S^{GEA} and F_S^{vW} may then be used to impose the von Weizsäcker bound, which is otherwise broken by the GEA at $z \leq -1$. Adapting a form recently used to construct a $\nabla^2 n$ -based exchange function [66] results in the enhancement factor

$$F_S^{mGGArev} = F_S^{vW} + 1 + zI(z), \quad (20)$$

where

$$I(z) = \{1 - \exp[-(1/|z|^\alpha)[1 - H(z)]]\}^{1/\alpha} \quad (21)$$

and H is the Heaviside step function. The interpolation function $I(z)$ is one for $z > 0$ and tends monotonically to $1/|z|$ as $z \rightarrow -\infty$, thus enforcing $F_S^{mGGArev} \rightarrow F_S^{vW}$ in this limit. Otherwise the functional mimics the GEA, which returns the slowly varying electron gas for $z \sim 0$, and has the correct scaling behavior for $z \rightarrow +\infty$ for a density exponentially decaying to zero. The differences between this approach and the mGGA are firstly the simplification of the functional used in the slowly-varying limit, a gradient expansion rather than a meta-GGA. Secondly the form of interpolator between slowly-varying and von Weizsäcker limits obeys a constraint that τ is greater than both τ_{GEA} and τ_{vW} while the mGGA interpolates *in between* the two limits. This difference proves to be helpful for modeling the KED of covalent bonds [47].

The factor α is used to control the rate at which the interpolating function switches between GEA and vW, with the leading correction to F_S^{vW} being

$$\lim_{z \rightarrow -\infty} F_S^{mGGArev} - F_S^{vW} \sim \frac{1}{z^\alpha}. \quad (22)$$

A factor of $\alpha = 1$ was considered in the original formulation; however this changes the value of the cusp in the kinetic energy density $(d\tau_{KS}(\mathbf{r})/dr)_{r=0}$ in the vicinity of a nucleus. For hydrogen, this can be shown to be exactly $-2Z/a_0$, but because the definition involves taking two derivatives of the particle density, this value is not universal. For small atoms it is identical to the cusp condition of the von Weizsäcker potential, but as discussed in the next section, it is altered for larger atoms by the occupation of p -orbitals which have a non-zero contribution to the KED at the nucleus. A safe choice may be $\alpha = 4$ which

does not contribute to the cusp of the KED and produces a Pauli potential that is zero at the nucleus. This is presumably the optimal choice for small atoms, like H where the Pauli KED should be small relative to the von Weizsäcker KED, but possibly not for larger atoms, as the Pauli contribution has to eventually become the dominant piece of the puzzle. Finally we note that this approach is not completely new – earlier work of Yang et al. [55] suggested a functional $\tau = \max(\tau_{vW}, \tau_{GEA})$, essentially the $\alpha \rightarrow \infty$ limit of the current model.

A. The Kohn-Sham kinetic energy density for atoms

The radial Kohn-Sham equation for an atom is

$$E_{nl}u_{nl}(r) = \left\{ \frac{1}{2} \left[-\frac{d^2}{dr^2} + \frac{l(l+1)}{r^2} \right] - \frac{Z}{r} \right\} u_{nl}(r), \quad (23)$$

where $u_{nl}(r) = rR_{nl}(r)$, n is the principle quantum number, l is the angular momentum quantum number, and $R_{nl}(r)$ is the radial wave function and r the radial distance from the nucleus. The KS density for a closed-shell, spherical atom is given by

$$n(r) = \sum_{l=0}^L \sum_{n=1}^N f_{nl} |R_{nl}(r)|^2, \quad (24)$$

where f_{nl} is the occupation number for the n, l subshell. This is strictly correct only for atoms with filled subshells, and we shall focus on two cases, the noble gases and alkali earths. The kinetic energy density for a spherical atom is

$$\tau_{KS} = \frac{1}{2} \sum_{l=0}^L \sum_{n=0}^N f_{n,l} \left[\left| \frac{dR_{n,l}(r)}{dr} \right|^2 + \frac{l(l+1)R_{n,l}(r)^2}{r^2} \right], \quad (25)$$

and the total kinetic energy is

$$T_{ks} = \int_0^\infty \tau_{ks}(r) d^3r. \quad (26)$$

1. Scaling to large Z

An elegant and systematic way of measuring the quality of approximate density functional theories is test their behavior for neutral atoms as the nuclear charge increases. In the case of hydrogen and helium, representing a limit of extreme electron localization, the KS functional reduces to the von Weizsäcker result. But as the nuclear charge increases, the core electrons of the atom behave more and more like a homogeneous electron gas. Thus, for an orbital-free density functional model to predict the kinetic energies of any atom, it must be able to predict accurately the transition between the homogeneity of extended systems to the extreme inhomogeneity of small

atoms and molecules. This would then make it a good candidate to replace the KS model for a variety of systems.

In the limit of large Z , the electronic structure of atoms tends exactly [26] to the Thomas-Fermi limit with total energy given by $E = -0.768745Z^{7/3}$. The density tends nearly everywhere to a universal smooth form, with quantum oscillations due to shell structure decreasing with amplitude as the number of shells increases [39]. The peak radial probability density occurs for $r = a_{TF}/Z^{1/3}$ with a close to a_B ; with this definition of atomic radius, the atomic radius scales as $Z^{-1/3}$. The Thomas-Fermi limit describes most accurately the core of the atom where the density is constructed from many interlacing orbitals and approaches a degenerate fermi gas. It must break down for the innermost shells since the Thomas-Fermi density unphysically diverges to infinity at $r=0$; it also breaks down at large r because the semiclassical approximation used to derive the Thomas-Fermi result cannot not describe classically forbidden regions. (In the latter case, the large- r limit of the density decays as $1/r^6$ rather than exponentially.)

The Thomas-Fermi energy is but the leading term in a general asymptotic expansion in Z [39]. For the kinetic energy this expansion is known for at least three terms:

$$T[Z] = AZ^{7/3} + BZ^2 + CZ^{5/3} + \dots \quad (27)$$

$A = 0.768745$ defines the Thomas-Fermi limit with $T = -E$ because of the virial theorem. $B = -0.5$ is the Scott correction [29, 32] which corrects the error in the Thomas-Fermi KE caused by the spurious divergence in the Thomas-Fermi density in the innermost shells of an atom. $C = 0.2699$ defines additional corrections derivable from the gradient-expansion correction to the Thomas-Fermi picture [33].

Finally we note that this asymptotic trend is an example of Lieb-Simon scaling [26, 27] where the potential is scaled by an arbitrary strength ζ , distance is scaled by $1/\zeta^{1/3}$, and the number of particles in the system is also scaled as ζ so that a charge-neutral system stays charge-neutral. This scaling procedure is defined as a generalization of the scaling which occurs as one goes down a column of the periodic table. As it defines the scaling of this perhaps most fundamental of all constructs in chemistry, it should be much more revealing than that of the normal uniform scaling to high density at fixed particle number.

For the purpose of this paper, we look for three regimes of density, the large- r asymptotic region $r > Z^{7/6}$, the core of the atom $r \sim Z^{-1/3}$ and the near-nuclear region $r < Z^{-2/3}$. We should expect a convergence to the Thomas-Fermi limit, and perhaps the gradient expansion for intermediate distances, but not for the other two regimes.

2. Limits

A number of facts are known about the KED in the limit of small and large r , and have recently been characterized in some detail [40]. As this region defines the leading error in the Thomas-Fermi picture, getting it right will be important to obtaining good kinetic energies. Although the density and thus KE density in the core of the atom tends to a finite value for $r \sim a_0/Z$ or less, the TF charge density diverges to infinity and the real charge density can never be treated by this approach. However, given the vanishingly small role of exchange and correlation in this limit, one may gain insight by modeling the density with orbitals taken from the hydrogen atom.

The charge density in this limit is given strictly by the contribution of $l=0$ orbitals. It has the cusp form [67] for small r :

$$\lim_{r \rightarrow 0} n(r) \rightarrow n(0)(1 - 2Zr/a_0) \quad (28)$$

with $n(0) \sim Z^3/a_0^3$. This fixes the $r=0$ value of the von Weizsäcker KED:

$$\lim_{r \rightarrow 0} \tau_{vW}(r) \rightarrow \frac{1}{2} \frac{Z^2}{a_0^2} n(0). \quad (29)$$

Taking the atomic KS KED defined above, we decompose into components from orbitals of specific angular momentum l and sum over all shells. For closed-shell atoms, we obtain

$$\tau_{KS} = \sum_l \sum_n \tau_{nl}. \quad (30)$$

At the nucleus, $r=0$, only the two lowest angular momentum components contribute: $l=0$ and $l=1$. The $l=0$ component of the KED is given by

$$\tau_0 = \sum_n f_{n0} |dR_{n0}/dr|^2 = \tau_{vW}. \quad (31)$$

The density at the nucleus $n(0)$ is constructed solely from the s orbitals and the probability density of each of these is of the form $n_{ns}(0)(1 - 2Zr/a_0)$. In other words, each orbital separately has the limiting cusp condition for the density defined above. This is enough to show that τ_0 is identical to the von Weizsäcker model result τ_{vW} .

The $l=1$ term comes from both non-zero centrifugal energy contribution to the KED and the square of the derivative of the radial orbital R_{n1} . It contributes a non-zero Pauli contribution to the KED at the nucleus for any atom with at least one occupied p orbital [54]. The resulting formula is

$$\tau_1 = \sum_n f_{n1} 3 |R_{n1}/r|^2 = \tau_{Pauli}. \quad (32)$$

As a result, we should expect to find that the $r=0$ limit of the KED and more specifically, the Pauli KED, to have a nontrivial dependence on the $l=1$ occupation number

and implicitly perhaps upon Z . It is worth noting that it has often been the assumption [38] that $\tau_{KS} \rightarrow \tau_{vW}$ in this limit. However the true non-zero value of the Pauli KED has long been known for atoms, and was part of the rationale behind the construction of functionals using the electron number N about an atom as an explicit functional variable [54]. The feature has recently been formally characterized and generalized to all central-potential problems [40], but it has yet to become part of an effective density functional.

Finally, the large- r limit of τ_{KS} follows from taking the contribution of the HOMO shell to the KED as $r \rightarrow \infty$. For a spherically symmetric atom (a closed shell atom or an open shell atom with uniform fractional occupancy), the result is [40]

$$\lim_{r \rightarrow \infty} \tau_{KS}(r) = \tau_{vW}(r) + \frac{l_H(l_H + 1)}{2r^2} n(r) \quad (33)$$

where l_H is the angular momentum quantum number of the HOMO shell, and the particle density $n(r)$ tends to that of the HOMO shell $n_{n_H, l_H}(r)$. It is notable that neither $|\nabla n|^2$ nor $\nabla^2 n$ preserves knowledge of the centrifugal force contribution to the KED. A radially symmetric density $n(r)$ is constructable without any reference to the angular components of the Kohn-Sham orbitals so that there is no way to generate terms that depend upon l . Thus we do not expect a good OFDFT model to the Pauli contribution to τ_{KS} in this limit.

III. METHODOLOGY

It is difficult to compare OFDFT models by solving them self-consistently. We rather solve the Kohn-Sham equation for a given system and use the resulting density for each model. To this end, we use the FHI98PP code [68] to generate Kohn-Sham particle and kinetic energy densities. FHI98PP is an atom code that computes Kohn-Sham orbitals on a logarithmic grid of potentially arbitrary accuracy for all particle radii. The formula for generating the grid is given by $r_{i+1} = \gamma r_i + r_0$ with $\gamma = 0.0247$. Because the well-known large- Z expansion is nonrelativistic, we do the same for our calculations to be able to make comparison. For simplicity, the local density approximation was used for calculating the exchange-correlation energy. This does not directly enter into the calculation of the kinetic energy or kinetic energy density, but might have some effect on the coefficients of the asymptotic expansion in Z .

To calculate the derivatives needed for calculating the KED and the Laplacian and gradient of the density on the logarithmic grid, we use a Lagrange-interpolation scheme which constructs approximate n -th order polynomials to be differentiated using $n+1$ grid points. A subgrid of thirteen points was found to be optimal, after dropping the first and last six points. Simpson's method was used for integrals.

Numerical and analytical tests to determine the accuracy of the differentiation and integration algorithms are described in Ref. [69]. The issue of replacing the exact density and LDA density may be assessed by comparing LDA kinetic energies for noble gases with those obtained using the optimized effective potential (OEP) method. These are shown in Table I. Notably, the percent error of the LDA diminishes rapidly for $Z > 10$, as it becomes asymptotically exact for infinite Z .

TABLE I. Errors in KS kinetic energies using the LDA density versus the OEP, from Ref. [39].

Atom	Z	T_S	T_{LDA}	% Error
He	2	2.86168	2.76739	3.295
Ne	10	128.545	127.737	0.629
Ar	18	526.812	524.967	0.350
Kr	36	2752.04	2747.81	0.154
Xe	54	7232.12	7225.09	0.097
Rn	86	21866.7	21854.7	0.055

IV. RESULTS

A. Visualizing a parameter space

Fig. 1 shows the main players for characterizing the kinetic energy density of a typical atom, Argon. Fig. 1(a) plots the scaled radial density versus scaled radius $Z^{1/3}r$. The peak of the Thomas-Fermi density, the $Z \rightarrow \infty$ limit, occurs at roughly $Z^{1/3}r = 0.3$ [39], in between the $n = 1$ and $n = 2$ shells; the shells oscillate above the TF peak value of ~ 0.38 . Fig. 1(b) shows suitably scaled values of p and q versus scaled radius. As noticed by Bader in the development of the QTAIM [70, 71], the Laplacian of the density, proportional to q , is negative (or more reliably, at a local minimum) at the centre of each shell, and is a local maximum in between shells. It tends to $-\infty$ at the nucleus because of the cusp in the electron density and to $+\infty$ far from the atom. The gradient variable p is finite at $r = 0$ but otherwise shows a similar behavior as q , with q lagging slightly behind it in a way reminiscent of sine and cosine functions.

We may gain more insight by plotting $q(r)$ versus $p(r)$, an analog to the phase-space plot $d\theta(t)/dt$ versus $\theta(t)$ encountered in the study of oscillator dynamics. The results for the first row of the periodic table, from Li through Ne, are shown in Fig. 2 and for the noble gases in Fig. 3. Comparing to Fig. 1(b), we can identify the three pertinent regions of the atom as three distinct features in “phase-space.” The classically-forbidden asymptotic region far from the nucleus shows up as a linear tail that extends to positive infinity in both p and q . The region near the nucleus characterized by the cusp in the electron density is the other end of each phase-space “trajectory”, where $q \rightarrow -\infty$ and p is finite and varies little with

Z . A system with only one shell, such as He in Fig. 3, transitions from the one region to the other seamlessly. Otherwise there is exactly one loop in p and q for every shell transition. The $n = 2$ to $n = 1$ or L to K shell transition is observable in Fig. 2; close observation of Fig. 3 reveals one loop for Ne, two for Ar, three for Kr and so on. The largest p and q values occur in the transition between shells, and the smallest at valence shell peaks. Thus in the midregion between the two extremes of cusp and asymptote, there is a tendency towards weak relative gradient corrections $p, q \ll 1$ – that is, towards the slowly-varying electron gas.

The trend to infinite Z in this picture is also revealing. The behavior of p and q in the cusp and asymptotic regions is essentially unchanging – there is only a modest shift from the He atom case to the largest Z atom. This may reflect the fact that neither of these two regimes can be adequately described in Thomas-Fermi theory: the charge density is singular at the nucleus and decays as $1/r^6$ as $r \rightarrow \infty$. One sees in some sense a renormalization of the trend described by the Helium atom – that is of the atomic features of the system furthest from the TF limit. It is in the core shells of the atom, which should eventually trend to the TF limit that a dependence upon Z is most clearly seen. The trend down the first row, shown in Fig. 2, is of the shell structure loop transitioning from an exceptionally large range of p and q for the smallest- Z atom, slowly towards the $p = q = 0$ limit. By Neon, the majority of the atom is within the range $p, q < 1$.

As further shells are added onto the system (Fig. 3), the space for any particular transition – L to K, M to L, N to M – consistently shrinks. Interestingly, the second innermost loop caused by the transition from the M to L shells rapidly shrinks to the perturbative regime $p, |q| \ll 1$ – one rapidly reaches the slowly-varying limit for inner shells as predicted by TF theory. However, the last transition, between K and L causes a large swing-out to higher p just before the trajectory transitions to the nuclear cusp. This may be indicative of the argument behind the Scott correction to the KE (the second term in Eq. 27) – that it involves not only the 1s shell, but contributions from the other innermost shells as well [32]. Focusing on the HOMO shell, the trend is less predictable but follows very gradually to the slowly-varying limit.

B. Parametric visualization of the kinetic energy density

Up to now only the visualization of the space defined by $p(\mathbf{r})$ and $q(\mathbf{r})$ has been discussed. We now include the Pauli enhancement factor of the Kohn-Sham KED, given by Eq. (14) in the third dimension. The result for the noble gases is shown as a scatter-plot over the numerical logarithmic grid in Fig. 4(a). This results in a three-dimensional parametric plot similar to the two-dimensional plot in Fig. 3. The view is rotated 30° about the z axis in Fig. 4(a) and 120° in (b).

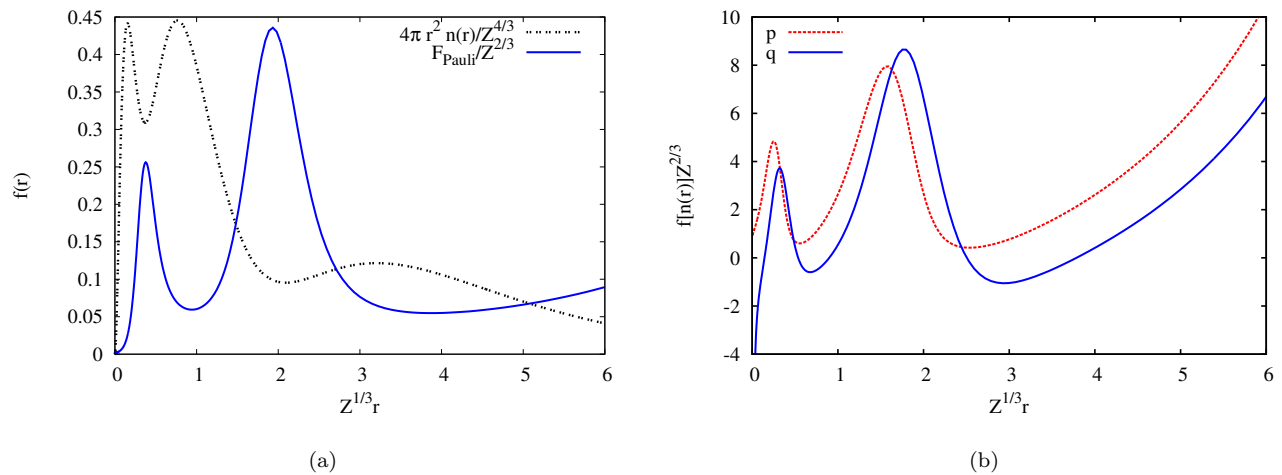


FIG. 1. (a) Scaled radial number density $n(r)$ and Pauli enhancement factor F_{Pauli} as a function of scaled radius $Z^{1/3}r$ for Argon. Scaling factors reflect scaling of atomic peak radius by $Z^{-1/3}$ and particle density by Z^2 for the Thomas-Fermi atom. (b) p (dotted line) and q (dashed) scaled by $Z^{2/3}$ and plotted as function of scaled radius.

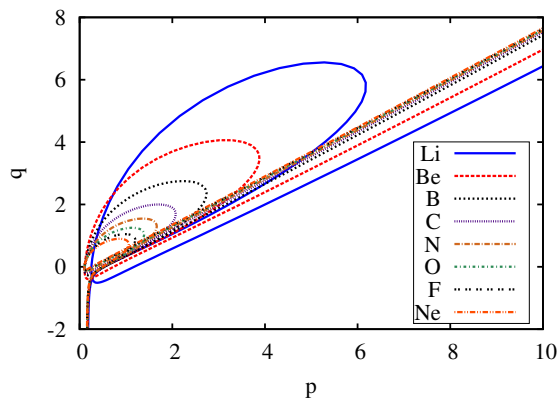


FIG. 2. Parametric plot of $p(r)$ vs $q(r)$ for row two of the periodic table.

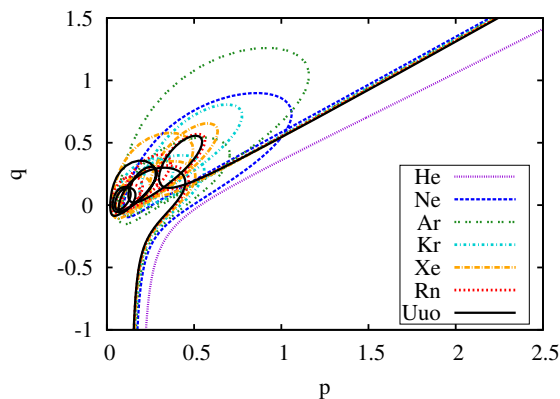


FIG. 3. Parametric plot of $p(r)$ vs $q(r)$ for all atoms in column VIII of the periodic table.

Note that He, shown as violet circles, has zero Pauli KED and thus lies entirely in the $F_{Pauli} = 0$ plane. All parametric curves start with a nearly universal behavior with $F_{Pauli} \sim 0$ near the nuclear cusp, shown as the tail for $p \sim 0$ and $q < 0$. The noble gases show approximately the same behavior for very large r , forming a second nearly universal curve. This however shows distinct signs of fanning out and is significantly different from He, or for other atoms, like Be, with no p frontier orbitals.

Most remarkably, it can be seen especially from (b) that the frontier and core regions of every atom are nearly coplanar. There is a perspective, not too far from that shown in (b) which looks at that plane edge on, in which the whole parametrized enhancement factor over all noble gases reduces to a simple hockey-stick form. This has several implications. For the observable range of values of p and q , F_{Pauli} for the noble atoms reduces to nearly a single-valued function of the two variables p and q . While either separately might lack sufficient information to characterize this set of systems, the combination does, and thus an unambiguous orbital-free functional may be constructed. But more than this: over much of its range, F_{Pauli} reduces to a simple linear function of the two. In terms of density functional theory, the Pauli enhancement factor is in large part that of a second-order gradient expansion. Finally, the region of the parameter space where the F_{Pauli} data does *not* fall into a plane is that of the cusp in the density near the nucleus, where a different universal behavior holds. The net result is that both regions can be described by a single parameter – a linear combination of p and q . The determination of this parameter and its use in modifying density functionals is described in the next sections.

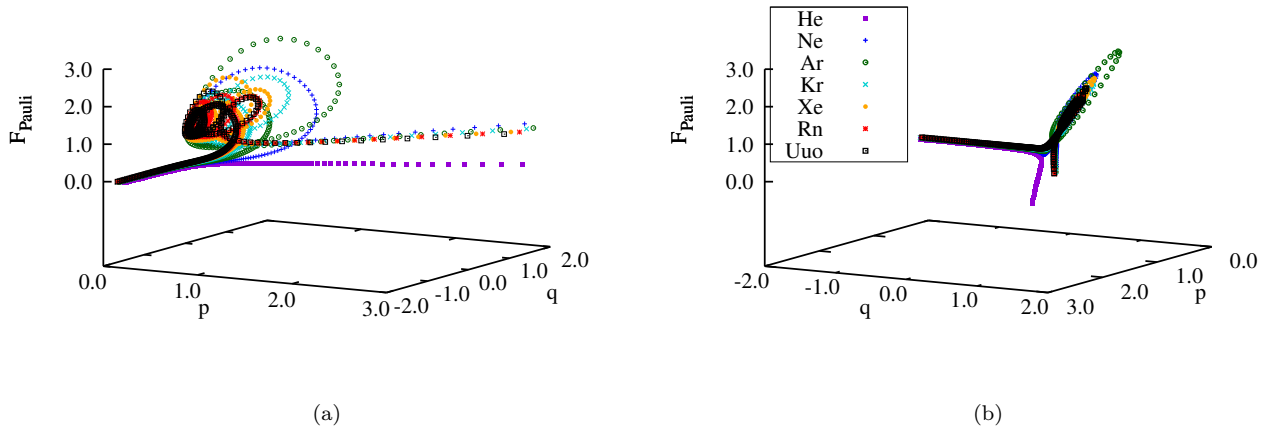


FIG. 4. (a) $F_{KS}^{Pauli}(\mathbf{r})$ versus $p(\mathbf{r})$ and $q(\mathbf{r})$ for noble gas atoms. Perspective is rotated 30 degrees about the z -axis with respect to the p -axis. (b) Same, for a 120 degree rotation.

C. Gradient Expansion Fits

We now assume the projection of F_{Pauli} onto a function defining a plane in p, q space. This describes a fit to a GEA:

$$F_{Pauli}^{GEAloc} = 1 + z_{loc} \quad (34)$$

with

$$z_{loc} = (a \cos \theta)p + (a \sin \theta)q \quad (35)$$

being an empirical version of the z variable introduced in Eq. (19). This defines a GE valid locally for the KE density rather than the normal GE, derived for the KE. Then a and θ can be determined by a least-squares-fit over a suitable range in p and q .

Ideally, given that the GEA should be most applicable in the limit $Z \rightarrow \infty$, we should take an extrapolation to the largest- Z atom numerically feasible. Such calculations of 1000's of electrons are chemically unrealizable but mathematically important for accurately determining limiting cases [11, 36]. Secondly, we should limit the range of the fit to values of $p, |q| \ll 1$, the range of validity for the gradient expansion.

A preliminary calculation shows that this may not be too important for our purposes. We perform a least squares fit of F_{Pauli} to Eqs. (34) and (35) for a given atom over all numerical grid points r_i for which $p(r_i) < 0.6$ and $-0.125 < q(r_i) < 0.6$. The results are shown for the alkali earths and noble gases in Fig. 5(a) for a and 5(b) for θ . The results converge very nearly to a constant for both columns after about $Z = 50$. Taking the last five atoms shown and averaging we get $a = 3.459(13)$ and $\theta = 2.1652(13)$. Taking the data for Uuo ($Z = 118$) only, and restricting the fit further to $p, q < 0.5$, we get $a = 3.486(26)$ and $\theta = 2.1615(28)$, a near match.

One point of interest here is that the values found empirically do not match those of the canonical [57] gradient expansion. The corresponding values of a and θ obtainable from Eq. (16), $a = 2.671$ and $\theta = 2.159$, are shown as straight lines in Fig. 5. Apparently, θ , measuring the relative mixture of p and q to the gradient expansion correction to the KED is unchanged to within statistical error. However the magnitude of the GE correction a converges quickly with Z to a value 30% larger than the predicted correction.

That is to say, the actual gradient expansion of the KE density, within the core region of the atom where this expansion is locally valid, is not the gradient expansion of the *integrated* KE.

The implications of this difference are quite dramatic. Convert these parameters back to the expression Eq. (11) for the KED and then to an expression for the total KE. We then get the following expressions for the result produced by the empirical local GEA for Uuo and the canonical GEA:

$$T^{GEA} = \int d^3r (1 + 0.185p + 2.222q)\tau_{TF} \quad (36)$$

$$T^{GEAloc} = \int d^3r (1 - 0.275p + 2.895q)\tau_{TF}. \quad (37)$$

Given that for a pure GEA functional, the GE term linear in q integrates to zero, the net GE contribution to the kinetic energy from the local GEA fit is the opposite sign from that of the canonical GE. As we shall see further on, it is actually the *wrong* sign – giving a GE expression for the energy that is worse than that for the Thomas-Fermi model.

It is also interesting that this is not the first evidence of such a qualitative discrepancy between the gradient expansions of the KE and KED. The recent analytic gradient expansion of the KED of the Airy gas [52], a system that asymptotically approaches an electron gas with

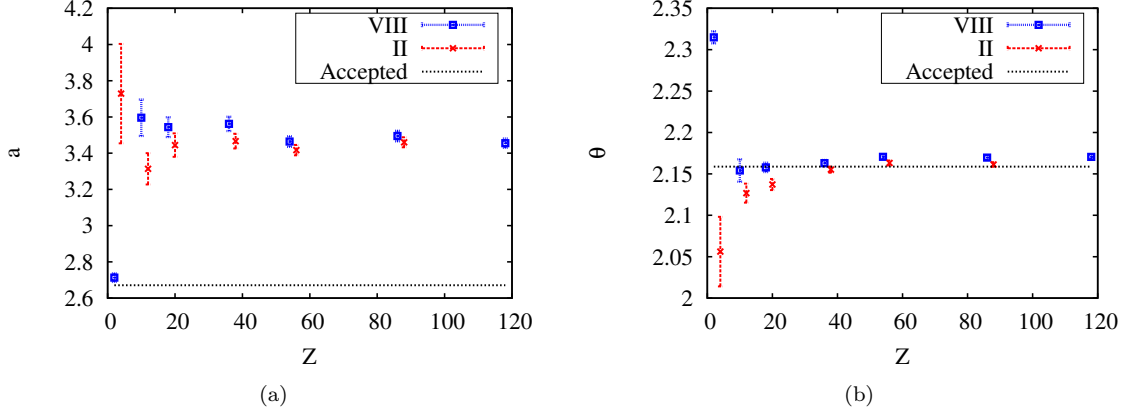


FIG. 5. (a) Fit parameter a and (b) fit parameter θ versus Z as determined by fitting Eqs. (34) and (35) to $F_{Pauli}^{KS}(p, q)$ for individual atoms. These are compared to values of a and θ from conventional gradient expansion (dotted line.)

a constant density gradient, also produces a negative coefficient for p . In this case, the kernel for the KE integral is $F_S = 1 - 0.185p + 3.333q$, which shows a similar change from the standard gradient expansion as that of the atom. However, quantitatively, these numbers are far outside the error bars of our statistical fits for the atom – the asymptotic limit of the KED of the neutral atom clearly tends to a different gradient expansion than that of the Airy gas. Nevertheless, it is reasonable to say that the gradient expansion about the local density approximation limit of a sloped system, either atom or Airy gas, is fundamentally different from that about the homogeneous electron gas.

D. Single-variable projection of the KED

We have seen that the behavior of F_{Pauli} for atoms projected upon the parameter space defined by $p(\mathbf{r})$ and $q(\mathbf{r})$ is capable of a great deal of simplification. Given the hypothesis that we might have a successful two-parameter parametrization $F_{Pauli}[p(r), q(r)]$, we find through Fig. 4 that we essentially only have a one-parameter space, $F_{Pauli}[z_{loc}(r)]$, with z_{loc} given by Eq. (35). The result is shown in Figs. 6 and 7.

These plots provide a wealth of detail that illuminate several key features of the Kohn-Sham KED of atoms. Most important of all is the visualization of how the KED scales to high Z . A single shell system such as He has zero Pauli KED and is in this sense infinitely far from the asymptotic limit. But any two-shell system already captures much of the sense of what happens at large Z , albeit with obvious shell structure – for example, F_{Pauli} for Ne (blue crosses) loops around but does not land on the GEA line. Here Be and Li, not shown, are worst cases, as one might expect, while Ne is already fairly close to the limit. As more and more shells are added, F_{Pauli} continues to loop around the large- Z asymptote defined by the GE line, but in ever tighter loops that rapidly

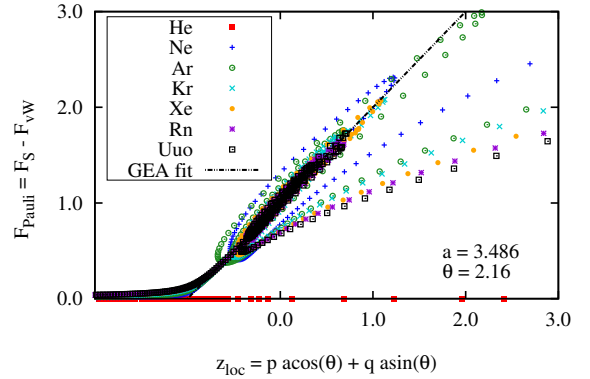


FIG. 6. $F_{Pauli}^{KS}(r)$ plotted parametrically versus $z_{loc}(r)$ [Eq. (35)] for the noble gas atoms, including Helium and Ununocium. Dashed line gives the GEA fit $F_{Pauli}^{GEAloc} = 1 + z_{loc}$. The values for a and θ used to define z_{loc} are those obtained by optimizing the fit for Uuo.

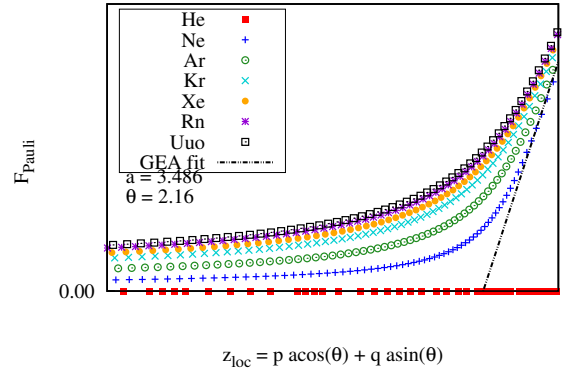


FIG. 7. The same as Fig. 6, but focusing on the near-nuclear regime where $q \rightarrow -\infty$.

approach the asymptote. There is a hint of curvature for Uuo that might imply a fourth-order gradient correction but a very small one, as is the case for the standard gradient expansion.

Second, we see the two regions that cannot be captured by Thomas-Fermi theory each demonstrate difficulties with the asymptotic model. First of all, the region $r \rightarrow \infty$ correlates with the loss of a well-defined single-valued function $F_{Pauli}(z)$. That is, for any point in the core region of an atom corresponding to some z_{loc} and some value of F_{Pauli} , there will be a point in the asymptotic region with the same value of z_{loc} but requiring a value of F_{Pauli} up to 50% smaller. Moreover, every individual atom seems to require a unique form for $F_{Pauli}(z)$ in the asymptotic region. Though the tails seem to converge to some finite value as Z increases, this convergence is also very slow.

This behavior may be an indication of the problem facing OFDFT in the asymptotic region discussed in Sec. II A 2. In this regime, the Pauli KED has a contribution from the HOMO shell [Eq. (33)] that depends upon the angular momentum quantum number of the shell. It therefore cannot be predicted from the total particle density alone. At the same time, it should be noted that the worst behavior occurs only for very large r . As seen in Fig. 1(a), the Pauli enhancement factor of the HOMO shell tends to be depressed relative to p and q and hovers around its minimum value for a fair distance. This is also seen as the clumping of a large number of grid points in Fig. 6 at the very last local minimum in F_{Pauli} before it trends off to ∞ . The impressive near-universal form seen in Fig. 4 is a reflection of the gradual onset of non-universal behavior.

A second difficulty occurs for the smallest radii, within the innermost shell of each atom, as shown in Fig. 7. Here the Pauli contribution to the KED is non-zero and measures the contribution of p -orbitals to the KED. Systems like He, Li and Be with no p -orbitals have exactly zero Pauli KED in this limit, as seen for He in this plot. For atoms with p orbitals, the result depends sensitively on how many shells are occupied, with the smallest F_{Pauli} for Neon and the largest for Uuo. There is a definite limiting case for infinite Z [40], which is approached rather slowly. The functional form of F_{Pauli} for these systems is linear in r at the nucleus – the enhancement factor has a finite cusp. This translates to a Pauli correction of the form $F_0(1 + A_0/z_{loc})$ where F_0 and A_0 necessarily depend upon the number of electrons. Although this seems to be a very small effect, with F_0 on the order of 0.02 for the largest physical atoms, it occurs in a limit with extremely high density and has a measurable impact upon integrated kinetic energies as we shall see in the next section.

E. Modified functionals for the KED

We find two insights for developing OFDFT from the perspective of the local kinetic energy density. First of all, rather than the canonical gradient expansion, which is derived to from an expression for the *integrated* kinetic energy of the slowly varying gas, we should start from the observed gradient expansion for the local kinetic energy density. In our mGGAreV model, this is achieved by simply replacing the argument z in Eq. (21) with z_{loc} of Eq. 35. This produces a new family of possible functionals (mGGALoc α) with different values of the parameter α that controls the rate at which the transition between gradient expansion and von Weizsäcker model occurs for strong electron localization. Analogous corrections can be made for the mGGA.

The second insight stems from the deviation of the KED from the gradient expansion near the nucleus. The nuclear region is a particular point of interest for models of the local KED such as the mGGA and the related meta-GGA's we have constructed. The transition to large negative values for the gradient expansion correction that occurs in this region breaks the basic constraint on the KED that $F_{Pauli} > 0$; in fact here $F_{Pauli}^{GEA} \rightarrow -\infty$. This region is thus necessarily a probe of the transition from the slowly-varying electron gas characterized by the GE and the localized electron limit dominated by the von Weizsäcker KED. Exactly how the Kohn-Sham KED responds in this situation is a clue as to how to model this transition.

The impacts of the varying strategies for doing this are shown in Fig. 8. This plots enhancement factors F_S for the special case of zero density gradient versus the Laplacian-based variable q . This limit is a fair approximation of the nuclear region, where p is small (< 0.2) and nearly constant while q tends to $-\infty$, as shown in Fig. 3. In this case, $\tau_{vW} = 0$ so that the lower bound it imposes is easy to visualize: $F_S = F_{Pauli} > 0$.

The canonical gradient expansion is shown to fourth order (dots), very nearly a straight line in q passing through the Thomas-Fermi limit $F_S = 1$ at $q = 0$. It very quickly goes below zero for negative q . The empirical local GEA (wider-spaced dots) exaggerates this behavior, given its steeper slope in q , evident in Eq. (37). The mGGA imposes $F_{Pauli} > 0$ by a sharp cutoff that interpolates between GEA and von Weizsäcker functionals in such a way as to be identically zero for negative q beyond the GEA crossover point. The mGGAreV [Eq. (21), with $\alpha = 1$] is shown as long-dashed line. This enforces $F_{Pauli} > F_{Pauli}^{GEA}$ which is beneficial for molecular bonding [47]. The short-dashed and dot-dashed lines show the mGGALoc with $\alpha = 1$ and $\alpha = 4$, which adhere to the local GEA outside the transition region.

Two points may be learned from this comparison. First of all, the functional form of the mGGAreV is closer to reality than that of the mGGA. As seen in Fig. 7 the KS KED tapers off like the blade of a hockey stick, as q and thus $z \rightarrow -\infty$, and certainly lacks the mGGA's abrupt

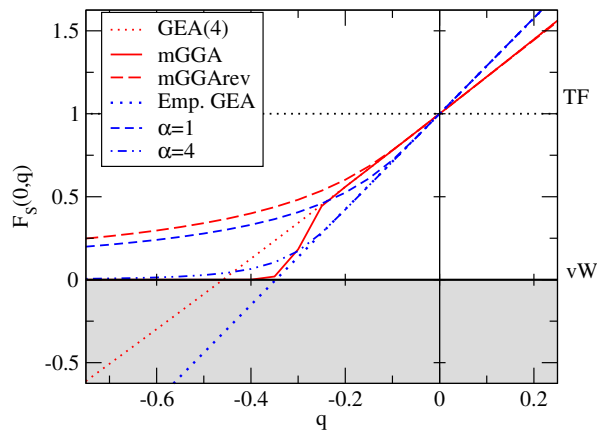


FIG. 8. The Pauli enhancement factor for the fourth-order GEA (dotted), meta-GGA’s based upon it (mGGA, mGGArev), and for the empirically fit second-order GEA (widely-spaced dotted) and variants of the mGGArev built upon it, using $\alpha = 4$ and 1 in Eq. 21. Shown versus q for $p = 0$, approximating the conditions near the atomic nucleus. Grey area shows region forbidden by the von Weizsäcker bound.

transition to zero. In that sense, the hypothesis upon which the mGGArev is based [47] – that $F^{KS} > F^{GEA}$ as $q \rightarrow -\infty$ – does hold here, as long as one uses the empirical *local* GEA, and not the canonical GEA.

However, as we shall see next, the mGGA is highly accurate for the total kinetic energy of atoms, while the mGGArev and its relation the mGGAloc1 give large overestimates. While having the correct qualitative shape, they both overestimate the contribution to the integrated KE from this region. Only the mGGAloc4 approaches the quality of the mGGA. The mGGA’s success thus seems to be from a clever weaving from the wrong gradient expansion limit, to the wrong approach to the von Weizsäcker limit in such a way as to cancel out the errors from each region. Getting a better local KED does not guarantee a better kinetic energy, thus meriting serious attention to the integrated quantity.

F. Integrated Kinetic Energy

Figures 9(a) and (b) show the integrated kinetic energy of the noble-gas atoms for many of the OFDFT models discussed in this paper, scaled by the Thomas-Fermi scaling factor $Z^{7/3}$ and plotted as a function of $Z^{-1/3}$. As discussed in Sec. II, the kinetic energy can be expressed as an expansion in powers of $Z^{-1/3}$, with the infinite- Z limit of $0.768745Z^{7/3}$ predicted by Thomas-Fermi theory. Also shown is a fit of the trend with Z for each functional to the asymptotic form [Eq. (27)]. The Thomas-Fermi limit is assumed for each case and the next two coefficients B and C are determined by linear regression over the noble gases excluding He. The fit coefficients and errors are shown in Table II.

The slight disagreement between the theoretical and

TABLE II. Least squares fit parameters for the Z expansion [Eq. (27)] of the noble gases for various OFDFT models of the kinetic energy. The Thomas-Fermi limit $A = 0.7687$ is assumed.

Model	B	C
Accepted	$-1/2$	0.2699
KS/LDA	-0.4943(43)	0.252(11)
TF	-0.649(7)	0.351(19)
GEA	-0.522(8)	0.292(20)
APBEK	-0.489(8)	0.241(21)
VT84F	0.116(20)	0.72(8)
mGGA	-0.493(9)	0.270(23)
mGGArev4	-0.429(7)	0.320(20)
GEAloc	-0.834(6)	0.437(16)
mGGAloc4	-0.618(5)	0.546(13)
fit4-NN	-0.4933(31)	0.273(5)

calculated asymptotic coefficients for the KS/LDA kinetic energy in Table II are within two standard deviations for the fit and thus seem reasonable. The errors due to the use of the LDA rather than exact KS density are probably much smaller.

Beyond this, it is possible to distinguish two classes of functionals. The canonical GEA obtained from the slowly-varying electron gas is already exceptionally close to the KS value and more sophisticated models like the mGGA struggle to improve upon or even do as well as it over all Z . Nevertheless, both it and the APBEK [11] are constructed in part through a fit to the large- Z limit. As a result both have excellent estimates of the asymptotic coefficients B and C and are nearly flawless for larger Z .

On the other hand, the mGGArev4, [Eq. (21) with $\alpha = 4$, labelled rev4 on the plot] is a serious regression, and the VT84F, whose asymptotic coefficients are shown in Table II, is worse. These have been constructed with constraint choices that emphasize the von Weizsäcker lower bound on the KED. In the mGGArev4 *and* in the VT84F, this is done by imposing the implicit constraint that $\tau > \max(\tau_{vW}, \tau_{GEA})$, the former by choice and the latter by necessity given the restricted flexibility of the GGA form. This leads to an overestimate of total energy, because the GEA is significantly less than the von Weizsäcker KED especially near the nucleus. Removing this unphysical behavior must cause a net increase in the total kinetic energy, whereas the GEA is already almost perfectly accurate. In contrast, the mGGA interpolates between slowly-varying and von Weizsäcker limit with a function that incorrectly obeys $\tau_{vW} < \tau < \tau_{GEA}$ – thus taking advantage of a natural cancellation of errors. Both of these effects are clearly seen in Fig. 10, which shows the radial KE density of the 1s shell of Neon. The GEA (dotted line) has a large negative error at the cusp, but an equally large error at the peak of the shell. In tran-

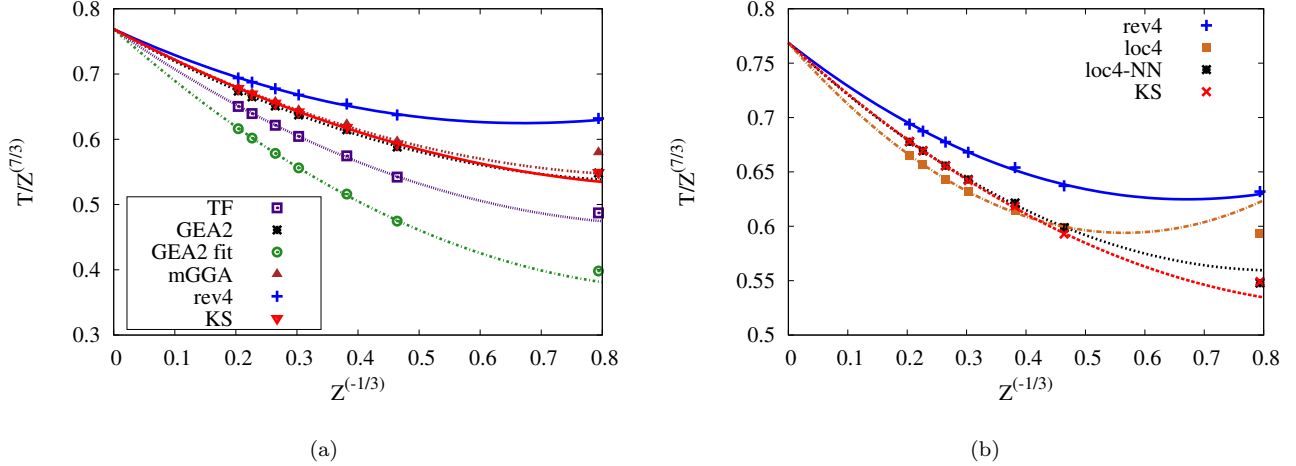


FIG. 9. (a) $T/Z^{7/3}$ versus $Z^{-1/3}$ for standard kinetic energy models discussed in the paper. GEA2-fit is the second-order GEA using empirical parameters of Eqs. (34) and (35). (b) the same, demonstrating the effect of using the empirical local GE in constructing OFDFT models.

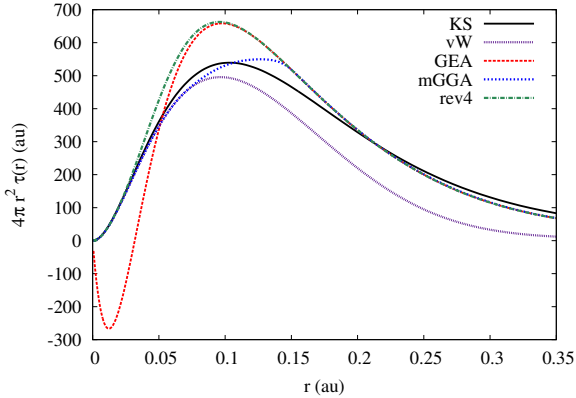


FIG. 10. (colour online) Kinetic energy radial densities in the 1s shell of the Ne atom.

sitioning from the GEA to the vW, the mGGA preserves this error cancellation. The mGGArev4 (dot-dashed line) fixes the error near the cusp but its constraint choice prevents it from fixing the error at the shell peak.

The final key to the story is the impact of the empirical local GEA we find for the KED. The impact of its deviation from the standard GEA is to lower the local KED with respect to it everywhere in the system. This produces a total KE that is much less even than the TF energy, as seen in Fig. 9. At the same time, this lowering of KED works naturally with the raising of energy caused by the imposition of the constraint $\tau > \tau_{vW}$ near the nucleus and the further constraint $\tau > \tau_{GEAloc}$ that we have observed throughout the 1s shell. The effect of combining this constraint with the local gradient expansion is shown in Fig. 9(b). While using the canonical gradient expansion with these constraints leads to the serious overestimate of the mGGArev4, the combination

of the right form of local gradient expansion with this constraint (labelled loc4) combine to almost cancel this error.

Unfortunately the overall quality of the asymptotic trend of the mGGAloc4 with Z is poor, as shown especially in Table II. This is the downside of the good cancellation of errors seen in the GEA: removal of one error-causing effect leads to poorer results unless the companion effect causing the cancellation is treated equally well. The problem here is the failure to account for the Pauli contribution from p orbitals in the near-nuclear region, which has a measurable effect on the quality of the answer. Thus a model for this effect is necessary, if only to understand the physics of the atom.

G. Empirical model of near-nucleus region

In the previous section we have taken as a reference model the revised mGGA of Eq. (21) with a transition parameter of $\alpha = 4$. This is a reasonable choice – it ensures that both the Pauli contribution to the KED and its potential $\delta\tau_{Pauli}(\mathbf{r})/\delta n(\mathbf{r})$ are zero near the nucleus. This ensures that for systems like He, for which there is no Pauli KED, or for small Z in general, that the near-nuclear region at least is handled reasonably. (It is improbable that a functional based upon the slowly-varying electron gas can produce zero τ_{Pauli} everywhere.) However, this choice of interpolating factor does not account for the non-zero contribution by p -orbitals to the Pauli KED at the nucleus. Unfortunately, we have seen (Table II and Fig. 9(b)) that our best empirical fit for the core and asymptotic regions gives a poor estimate for integrated KE's of atoms. This indicates that the error in ignoring the Pauli contribution to the KED near the nucleus is a measurable effect. Though the Pauli enhance-

ment factor in this region is small (Fig. 7), it results in a significant contribution to the KE given the enormous densities for large- Z atoms. And unfortunately, we need a correction that is different for every row of the periodic table, each of which adds a new p orbital to the system and an additional contribution to the Pauli KED. Thus a correction to the von Weizsäcker KED is required for this region that is somehow dependent upon the electron number N .

As a first step in this direction, we build upon the N -dependent model developed by Acharya et al. [54] Their work noted that an excellent model of the KED for atoms could be obtained by first taking a slowly-varying model of the KED such as the TF or GEA model for all shells but the innermost K shell. Then, for the K shell, the model is replaced by the von Weizsäcker KED:

$$\tau[n] = \tau_0[n] - \tau_0[n_K] + \tau_{vW}[n_K] \quad (38)$$

with τ_0 the KED of the initial slowly-varying model and n_K the density of the K-shell. Note that at the nucleus this model essentially restricts τ_0 to the description of the small Pauli contribution to the KED due to p orbitals, and assumes that τ_{vW} contributes negligibly elsewhere. With reasonable assumptions about the nature of the K shell density n_K , one gets an N -dependent model for the KE:

$$T[n] = \frac{T_{vW}[n] + T_0[n]}{1 + c/N^{1/3}}. \quad (39)$$

A very similar approach has recently been proposed [42] which uses the KED of the K-shell as a basic variable for building an OFDFT and extending the analysis to treat the exchange contribution from this shell. It provides excellent predictions of exchange and kinetic energy densities near the nucleus, suggesting that the careful treatment of the K-shell density is the key to modeling the KED in this region. We will take another tack to this issue, by determining an N -dependent correction to the mGGArev functional that reproduces the important features of the Acharya KED in the near-nuclear regime and recovers the asymptotic scaling of the KE of atoms to large Z . We do so by modifying the mGGArev interpolation function $I(z)$, using $z = z_{loc}$, to

$$I_{NN}(z_{loc}, N) = \{1 - \exp[-\beta^\alpha(N)/|z_{loc}|^\alpha]H(-z_{loc})\}^{1/\alpha} \quad (40)$$

where

$$\beta(N) = A_{NN} + \frac{B_{NN}}{N^{1/3}}. \quad (41)$$

Expanding about the near-nuclear limit $z_{loc} \rightarrow -\infty$ we find

$$\lim_{z \rightarrow -\infty} F_S^{mGGArev} = F_S^{vW} + 1 - \beta. \quad (42)$$

Essentially, the correction contributes a non-zero component to Pauli KED in the near-nuclear region with the

same scaling in N as the empirical Acharya correction. By adjusting the constants A_{NN} and B_{NN} , our functional can be empirically fit to the Z scaling behavior of the KS KE for large Z atoms. Our original model is recovered with $A_{NN} = 1, B_{NN} = 0$. Values of $A_{NN} \approx 0.77$ and $B_{NN} \approx 0.50$ give a nearly ideal fit to the Kohn-Sham kinetic energy as seen in Fig. 9(b). These are remarkably close to the large- Z expansion parameters of Eq. (27), although we have no evidence that this is more than a coincidence.

Nevertheless, these values are poor predictors of the actual KED at the nucleus – while the actual value of $F_{Pauli}(r=0) \sim 0.022$ at the nucleus for Rn, our correction predicts a value six times larger. This is indicated by error introduced into the KED as $r \rightarrow 0$, as seen for Argon in Fig. 11(a) and Uuo in Fig. 11(b). The excellent KE's are caused by successful cancellation of errors between those of the near-nuclear regime and that accumulated across the rest of the atom. Interestingly, the need is to make the fit in the near-nuclear region worse compared to the non- N -dependent mGGAloc model. By comparing Fig. 11(a) to Fig. 1(a), we find the second largest source of error for the mGGAloc4 (fit-4 in the plot) comes in the transition between shells, where F_{Pauli} has a local maximum. This error is already outside the nuclear cusp region and in that of oscillatory behavior of F_{Pauli} about the gradient expansion asymptote as seen in Fig. 6. As Z increases, the magnitude of the error increases, and more shells seem to be involved, but its contribution to the total KE decreases, as the region of error moves farther from that of peak radial charge density at $Z^{1/3}r \sim 1$. Fig. 11 tells roughly the same story for the mGGA, and the cancellation of error in that model, but with generally larger amplitude oscillations.

V. DISCUSSION AND CONCLUSIONS

We have analyzed scaling trends in the positive-definite Kohn-Sham kinetic energy density over the periodic table of atoms. We have concentrated our attention to the transition to the large- Z limit, in order to characterize the diminishing size of the corrections to the Thomas-Fermi limit as Z increases. Second-order density derivatives $\nabla^2 n$ and $|\nabla n|^2$ expressed in scale-invariant form provide a intuitively useful and nearly complete visual description of the atom and particularly, the trends with Z of different local regions of the atom – nucleus, core, and valence shell. The pair thus should be a useful basis for constructing orbital-free maps of local quantities such as the kinetic energy density or the energy densities associated with the exchange and correlation holes.

In fact, we find that over much of the atom, corresponding roughly to the regime of validity of the TF model in the infinite- Z limit, the Kohn-Sham KED is exceptionally well fit by a simple second-order gradient expansion. For low Z deviations from this asymptotic trend, caused by shell structure, naturally oscillate about

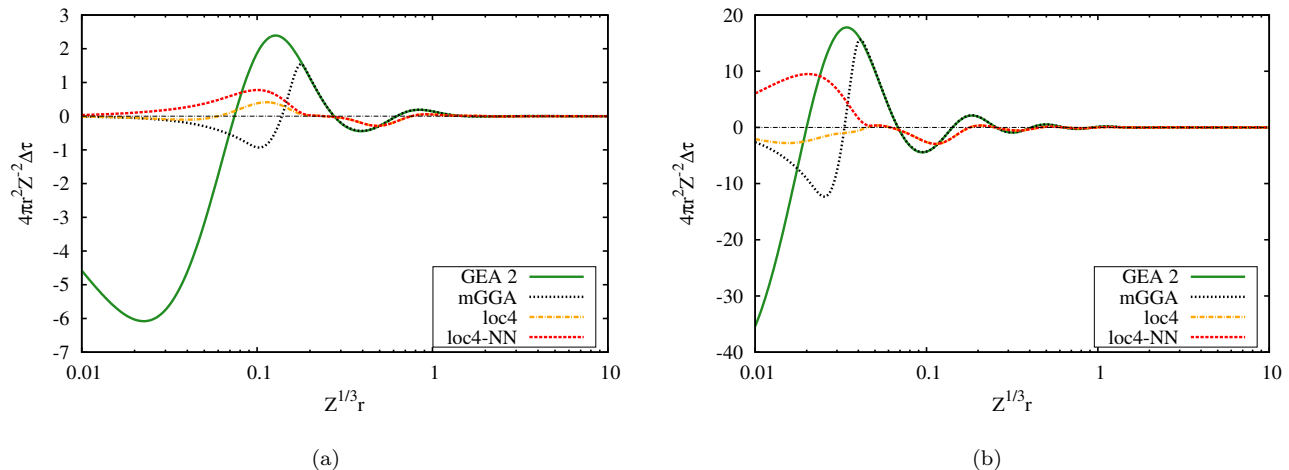


FIG. 11. (a) Error in the scaled radial KED of Argon $4\pi r^2[\tau_{model}(\mathbf{r}) - \tau_{KS}(\mathbf{r})]/Z^2$ versus scaled radius for several KED models. (b) The same, for ununocium ($Z=118$).

it and gradually reduce as Z increases. At large Z , the local GE model becomes nearly exact, and independent of column. This suggests that the gradient expansion is the fundamental semilocal density functional correction to the TF limit, but with the significant caveat that the local gradient expansion for the KED is not the global one for the KE. In fact it is qualitatively different – the correction to the integrated Thomas-Fermi KE obtained from the local gradient expansion is the opposite sign of the normal case. Thus, we cannot say that if $T_{KS} = \int \tau_{model}(\mathbf{r})d^3r$ then $\tau_{KS}(\mathbf{r}) = \tau_{model}(\mathbf{r})$, or vice-versa. Note that this is not simply an issue of choice of “gauge”, where one might compare two KED’s defined in alternate ways that integrate to the same value. In this paper, only the unique positive-definite gauge is used.

Rather the problem is fundamental – the relative success of Kirzhnits GE is not because of the accuracy of the underlying local functional $\tau[n(\mathbf{r})]$ because this breaks the lower bound $\tau > \tau_{vW}$. It rather captures a cancellation of errors in the integral of τ – the breaking of the von Weizsäcker lower bound near the nucleus being compensated by an overestimate of the local gradient correction elsewhere. This points to the much greater difficulty in modeling the local versus the global quantity, as the former requires modeling from point to point and is thus much less amenable to beneficial error cancellation. At the same time these results confirm, qualitatively if not quantitatively, the gradient expansion analysis of Ref. [52] for the Airy gas, a model designed asymptotically to represent a system that is all surface. Together these two asymptotic limits strongly suggest that the Kirzhnits gradient expansion should not be used in an application (presumably including bonding) that would depend sensitively on the local kinetic energy density.

It is not surprising to find that the greatest difficulties in removing this point-to-point error using the second-order gradient quantities p and q are the two limits in

which Thomas-Fermi theory fails. The asymptotic limit far from the atom is problematic because the Pauli kinetic energy deviates from being a single-valued function of these variables. This seems to be related to the dependence of τ_{KS} on the angular momentum number l_{HOMO} of the HOMO orbital [40], something that is not predictable with only $\nabla^2 n$ or $|\nabla n|^2$. The use of higher-order derivatives might help in this case [61]. The near-nuclear region dominated by the cusp in the density is also difficult because of the sensitive dependence of the Pauli KED on the number of electrons occupying p -orbitals in the system. This might be crudely approximated with the reduced density gradient p , which also shows a weak dependence on N , but the recent nonlocal approach of Ref. [42] should be more robust.

In all then, it is not surprising that a simple fix to our OFDFT meta-GGA models, replacing the global gradient expansion with the empirical local one we find here, fails to produce good total kinetic energies for the atoms. While they can hit the ballpark of KS energies, they do not compare favorably even to the lowest level conventional gradient correction. Rather our findings should help to develop OFDFT models that much more accurately model the KED in the bulk of the atom than prior models. In this, the fact that we can limit the functional to a gradient expansion and not a GGA helps a lot – a gradient expansion has a well behaved Pauli potential that neither breaks known constraints nor generates unphysical oscillatory behavior.

At the same time, we can reproduce the integrated KE of atoms with excellent accuracy given a fit to a simple N -dependent modification of our orbital-free model. A density-functional theory that depends upon the number of electrons N may be less than satisfactory from an *a priori* standpoint. More to the point perhaps is that this close fit is achieved by introducing, not reducing, error into the KED at the nucleus in order to can-

cel out the net error from inner shells. A connection to semiclassical theory may explain this. In a paper deriving the Scott correction $B = -1/2$ to the Thomas-Fermi KE [32], Schwinger noted that the correction came not just from the cusp region where the Thomas-Fermi density diverges, but also from quantum oscillations in the inner shells – those with peaks at radii $r_{peak} \ll Z^{1/3}a_B$. In our situation, for even the largest system, Uuo, we see not only large errors at the nucleus, but in the quantum oscillations about the gradient expansion that damp out only gradually. We believe that for $Z \rightarrow \infty$ these oscillations will remain large for any atom, but extending only over a fraction of the inner shells, becoming negligible relative to the total energy. The point is that a successful model of the KED for atoms will have to account for both the unusual Pauli energy density *at* the nucleus and for large quantum oscillations in the nearby shells. The progress made to handle the former in Ref. [42] will need to be matched by improvement in the latter; these might be made by a fourth-order gradient correction.

A final issue is whether the use of a negative gradient correction in the gradient expansion helps to improve binding energies predictions for molecules, or perhaps

makes them worse. This issue is currently being explored. Preliminary data for the AE6 test set show that the use of a mGGALoc using the atomic local GEA rather than a mGGAreV using the conventional GEA does improve binding energies consistently. At the same time, the indication is that this improvement is nowhere near enough to make OFDFT competitive with Kohn-Sham methods. However, it would be interesting to explore the effect of the use of a negative gradient expansion coefficient in a GGA. If the best performer on the test set, the VT84F, showed a similar improvement in binding energy we see for our meta-GGA's, it should come within the ballpark of the LDA in performance. Our findings thus should make a contribution, if not a decisive one, towards solving the challenge of the orbital-free prediction of covalent bonding.

ACKNOWLEDGMENTS

A.C.C would like to thank Kieron Burke and Sam Trickey for useful discussions.

-
- [1] P. Hohenberg and W. Kohn, Phys. Rev. **136**, B864 (1964).
 - [2] V. Karasiev, D.Chakraborty, and S. Trickey, in *Many-Electron Approaches in Physics, Chemistry, and Mathematics*, edited by L. D. Site and V. Bach (Springer Verlag, Berlin, 2013).
 - [3] A. V. Akimov and O. V. Prezhdo, Chemical Reviews **115**, 5797 (2015), pMID: 25851499.
 - [4] F. Graziani, ed., *Frontiers and Challenges in Warm Dense Matter* (Springer Verlag, Berlin, 2014).
 - [5] *Basic Research Needs for High Energy Density Laboratory Physics: Report on the Workshop on High Energy Density Laboratory Physics Research Needs, Nov. 1518, 2009*, Tech. Rep. (Dept. of Energy).
 - [6] A. D. Becke, Phys. Rev. A **38**, 3098 (1988).
 - [7] C. Lee, W. Yang, and R. G. Parr, Phys. Rev. B **37**, 785 (1988).
 - [8] J. P. Perdew, K. Burke, and M. Ernzerhof, Phys. Rev. Lett. **77**, 3865 (1996); **78**, 1396(E) (1997).
 - [9] V. V. Karasiev, D. Chakraborty, O. A. Shukruto, and S. B. Trickey, Phys. Rev. B **88**, 161108 (2013).
 - [10] V. V. Karasiev, R. S. Jones, S. B. Trickey, and F. E. Harris, Phys. Rev. B **80**, 245120 (2009).
 - [11] L. A. Constantin, E. Fabiano, S. Laricchia, and F. Della Sala, Phys. Rev. Lett. **106**, 186406 (2011).
 - [12] F. Tran and T. A. Wesolowski, Int. J. Quantum Chem. **89**, 441 (2002).
 - [13] D. J. Lacks and R. G. Gordon, J. Chem. Phys. **100**, 4446 (1994).
 - [14] A. Thakkar, Phys. Rev. A **46**, 6920 (1992).
 - [15] L. H. Thomas, Math. Proc. Camb. Phil. Soc. **23**, 542 (1927).
 - [16] E. Fermi, Zeitschrift für Physik A Hadrons and Nuclei **48**, 73 (1928).
 - [17] V. V. Karasiev, S. B. Trickey, and F. E. Harris, Journal of Computer-Aided Materials Design **13**, 111 (2006).
 - [18] H. Lee, C. Lee, and R. Parr, Phys. Rev. A **44**, 768 (1991).
 - [19] L.-W. Wang and M. Teter, Phys. Rev. B **45**, 13196 (1992).
 - [20] Y. Wang, N. Govind, and E. Carter, Phys. Rev. B **60**, 16350 (1999).
 - [21] Y. Wang, N. Govind, and E. Carter, Phys. Rev. B **64**, 089903 (2001).
 - [22] C. Huang and E. Carter, Phys. Rev. B **81**, 045206 (2010).
 - [23] Y. Ke, F. Libisch, J. Xia, and E. A. Carter, Phys. Rev. B **89**, 155112 (2014).
 - [24] L. Hung and E. A. Carter, J. Phys. Chem. C **115**, 6269 (2011).
 - [25] I. Shin and E. A. Carter, Phys. Rev. B **88**, 064106 (2013).
 - [26] E. H. Lieb and B. Simon, Adv. in Math. **23**, 22 (1977).
 - [27] E. Lieb and B. Simon, Phys. Rev. Lett. **31**, 681 (1973).
 - [28] L. Spruch, Reviews of Modern Physics **63** (1991).
 - [29] J. M. C. Scott, Philos. Mag. **43**, 859 (1952).
 - [30] N. H. March and J. S. Plaskett, Proceedings of the Royal Society A **235**, 419 (1956).
 - [31] N. H. March and R. G. Parr, Proc. Natl. Acad. Sci. USA **77**, 6285 (1980).
 - [32] J. Schwinger, Phys. Rev. A **22**, 1827 (1980).
 - [33] B.-G. Englert and J. Schwinger, Phys. Rev. A **32**, 26 (1985).
 - [34] B.-G. Englert and J. Schwinger, Phys. Rev. A **26**, 2322 (1982).
 - [35] P. Elliott and K. Burke, Canadian Journal of Chemistry **87**, 1485 (2009).
 - [36] K. Burke, A. Cancio, T. Gould, and S. Pittalis, (2016), arXiv:1602.08546.
 - [37] K. Burke, A. Cancio, T. Gould, and S. Pittalis, (2014), arXiv:1409.4834.

- [38] J. P. Perdew, A. Ruzsinszky, G. I. Csonka, O. A. Vydrov, G. E. Scuseria, L. A. Constantin, X. Zhou, and K. Burke, *Phys. Rev. Lett.* **100**, 136406 (2008).
- [39] D. Lee, L. A. Constantin, J. P. Perdew, and K. Burke, *The Journal of chemical physics* **130**, 034107 (2009).
- [40] F. Della Sala, E. Fabiano, and L. A. Constantin, *Phys. Rev. B* **91**, 035126 (2015).
- [41] S. Laricchia, L. A. Constantin, E. Fabiano, and F. D. Sala, *Journal of Chemical Theory and Computation* **10**, 164 (2014).
- [42] L. A. Constantin, E. Fabiano, and F. Della Sala, *Computation* **4** (2016), 10.3390/computation4020019.
- [43] A. D. Becke and K. E. Edgecombe, *J. Chem. Phys.* **92**, 5397 (1990).
- [44] B. Silvi and A. Savin, *Nature (London)* **371**, 683 (1994).
- [45] A. D. Becke, *J. Chem. Phys.* **109**, 2092 (1998).
- [46] J. Sun, B. Xiao, Y. Fang, R. Haunschild, P. Hao, A. Ruzsinszky, G. I. Csonka, G. E. Scuseria, and J. P. Perdew, *Phys. Rev. Lett.* **111**, 106401 (2013).
- [47] A. Cancio, D. Stewart, and A. Kuna, *Journal of Chemical Physics* **144**, 084107 (2016).
- [48] K. Finzel, *Theoretical Chemistry Accounts* **134**, 106 (2015).
- [49] J. Xia and E. A. Carter, *Phys. Rev. B* **91**, 045124 (2015).
- [50] S. B. Trickey, V. V. Karasiev, and D. Chakraborty, *Phys. Rev. B* **92**, 117101 (2015).
- [51] J. Xia and E. A. Carter, *Phys. Rev. B* **92**, 117102 (2015).
- [52] A. Lindmaa, A. E. Mattsson, and R. Armiento, *Phys. Rev. B* **90**, 075139 (2014).
- [53] J. P. Perdew and L. A. Constantin, *Phys. Rev. B* **75**, 155109/1 (2007).
- [54] P. K. Acharya, L. J. Bartolotti, S. B. Sears, and R. G. Parr, *Proc. Natl. Acad. Sci. USA* **77**, 6978 (1980).
- [55] W. Yang, R. G. Parr, and C. Lee, *Phys. Rev. A* **34**, 4586 (1986).
- [56] R. O. Jones and O. Gunnarsson, *Rev. Mod. Phys.* **61**, 689 (1989).
- [57] D. Kirzhnits, *Sov. Phys. JETP* **5**, 64 (1957).
- [58] M. Brack, B. K. Jennings, and Y. H. Chu, *Phys. Lett.* **65B** **65**, 1 (1976).
- [59] C. H. Hodges, *Can. J. Phys.* **51**, 1428 (1973).
- [60] D. Murphy, *Phys. Rev. A* **24**, 1682 (1981).
- [61] P. de Silva and C. Corminboeuf, *J. Chem. Phys.* **143** (2015), <http://dx.doi.org/10.1063/1.4931628>.
- [62] C. Weizsäcker, *Zeitschrift für Physik* **96**, 431 (1935).
- [63] C. Herring, *Phys. Rev. A* **34**, 2614 (1986).
- [64] M. Levy and H. Ou-Yang, *Phys. Rev. A* **38**, 625 (1988).
- [65] F. Hao, R. Armiento, and A. E. Mattsson, *J. Chem. Phys.* **140**, 18A536 (2014).
- [66] A. C. Cancio and C. E. Wagner, (2013), arXiv:1308.3744 [physics.chem-ph].
- [67] T. Kato, *Commun. Pure Appl. Math.* **10**, 151 (1957).
- [68] M. Fuchs and M. Scheffler, *Computer Physics Communications* **119**, 67 (1999).
- [69] J. J. Redd, Master's thesis (2015).
- [70] R. F. W. Bader, *Chemical Reviews* **91**, 893 (1991).
- [71] R. F. W. Bader and H. Essén, *J. Chem. Phys.* **80**, 1943 (1984).